PERGAMON

Deep-Sea Research I 48 (2001) 567–591

DEEP-SEA RESEARCH
PART I

www.elsevier.com/locate/dsr

Cross-slope zonation of erosion and deposition in the Faeroe-Shetland Channel, North Atlantic Ocean

Wim van Raaphorst*, Hans Malschaert, Hans van Haren, Wim Boer, Geert-Jan Brummer

Netherlands Institute for Sea Research (NIOZ), PO Box 59, 1790 AB Den Burg, Netherlands

Received 7 September 1999; received in revised form 24 February 2000; accepted 27 April 2000

Abstract

Boundary currents and internal waves determine cross-slope zonation of erosion and deposition in the Faeroe-Shetland Channel. Currents were measured at 8 and 34–50 m above the bottom at three mooring sites (502, 595 and 708 m depth) for 14 days. The structure of the water column was evaluated from CTD sections, and included nepheloid layers and particulate matter concentrations. Indicators for recent deposition in the sediment (organic carbon, phytopigments, ^{210}Pb) were measured at eight stations across the slope. Strong near-bottom currents at the upper slope sustain down-slope particle transport in a benthic nepheloid layer, which is eroded under the influence of critically reflecting M_2 internal tidal waves at 350–550 m, where the major pycnocline meets the sloping bottom. Beam attenuation profiles confirmed the presence of intermediate nepheloid layers intruding into the Channel along the major pycnocline, and elevated concentrations of particulate matter and chlorophyll-*a* were measured at this depth. Near-bottom currents decreased with depth, thus allowing particle deposition down the slope. Inventories of excess ^{210}Pb activity in the sediment deeper than 600 m were higher than what was expected on the basis of atmospheric input of ^{210}Pb and production in the water column, thus indicating additional lateral inputs. Simple calculations showed that off-slope input of particles from areas shallower than 600 m may be responsible for the enhanced deposition at greater depths.

Keywords: Continental slope; Internal waves; Nepheloid layer; Suspended particulate matter; Sedimentation; North Atlantic Ocean; Faeroe-Shetland Channel; 60°30′N 2°W–61°30′N 5°W

1. Introduction

Continental slopes constitute important and complex regions connecting shallow shelf seas and the deep ocean. Although continental margins contribute only about 11% to the surface area of the

* Corresponding author. Fax: 31-0-222-319674.
E-mail address: wimvr@nioz.nl (W. van Raaphorst).

0967-0637/01/$ - see front matter
PII: S0967-0637(00)00052-2

world ocean, over ~20% of the global primary production takes place there (Wollast, 1991). Large multidisciplinary research programs have been conducted in the recent past to determine the exchange fluxes from the productive shelf to the deep ocean, e.g. SEEP I (Walsh et al., 1988) and SEEP II (Biscaye et al., 1994) in the Middle Atlantic Bight, ECOMARGE in the Gulf of Lions (Monaco et al., 1990) and OMEX I at the Goban Spur on the NW European margin (Van Weering et al., 1998). All these programs have indicated that cross-slope advection contributes substantially to the flux of biogenic debris to the sediments on the slope.

The main source of nepheloid layers, in which much of the cross-slope particle transport above continental slopes occurs (Puig and Palangues, 1998), is sediment resuspension at the outer shelf, the shelf break and the upper slope (Biscaye and Anderson, 1994; Van Weering et al., 1998; Monaco et al., 1999; Durrieu de Madron et al., 1999a). In the Middle Atlantic Bight particles are either flushed away with the along-slope current or deposited in a mid-slope depocentre (Walsh et al., 1988; Biscaye et al., 1994) where the turbulent kinetic energy density in the bottom water is at minimum (Csanady et al., 1988). Distinct depocentres on the slope were not found in the Goban Spur (Lohse et al., 1998; Van Weering et al., 1998) or the Gulf of Lions (Courp and Monaco, 1990), but sediment deposition rates were not evenly distributed across the slopes in these areas, either.

Strong boundary currents may be the cause of erosion at the upper slope and the shelf break (e.g. Thomsen and Van Weering, 1998; Durrieu de Madron et al., 1999b). Heavy storms over the outer shelf (Churchill et al., 1994; Brunner and Biscaye, 1997), internal waves impinging from the ocean on the slope (Cacchione and Drake, 1986; Dickson and McCave, 1986; Thorpe and White, 1988; Atzetsu-Scott et al., 1995; Durrieu de Madron et al., 1999a), and combinations of these processes (Huthnance, 1995) are likely causes also. Recently, direct turbulence measurements around a sub-surface seamount have revealed bands of enhanced turbulence dissipation levels emanating from the sloping bottom (Lueck and Mudge, 1997). Where these bands, corresponding to ray-paths of internal waves, meet the seafloor, erosion of the bottom nepheloid layer (BNL) may occur to form an intermediate nepheloid layer (INL) extending off the slope. Increased turbulence above a slope and the resulting formation of INLs has been attributed to critical internal wave reflection (Dickson and McCave, 1986; Thorpe and White, 1988). Geometric focusing of internal waves along distinct attractor beams allowing repeated reflections may be an alternative mechanism (Maas et al., 1997). Critical reflection and geometric focusing of internal waves both can cause sediment erosion in restricted, but different, depth zones on the slope and re-deposition at greater depth where near-bottom turbulence is sufficiently less.

Here, we report results from the PROcesses on the Continental Slope (PROCS) pilot program in the Faeroe-Shetland Channel (North Atlantic Ocean) during May 1997. Previous work in this area focused on the complicated hydrography (Van Aken and Eisma, 1987; Van Aken, 1988; Turrell et al., 1999), large-scale dispersion (Burrows et al., 1999) and the dynamics of eddies (Oey, 1998). Sherwin (1991) evidenced occurrence of internal waves. Less information exists on the patterns of erosion and deposition in the Channel, though the general composition of the surficial sediments is well-described (Stoker et al., 1993). The overall objectives of PROCS were to investigate whether internal wave focusing is a major cause for the mixing of the stratified water column over the sloping bottom of the channel and if the impact of reflecting internal waves can be traced in the sediment. This paper deals with the second part of these objectives with its main emphasis on the suspended and near-surface seabed sediments. Others will discuss the issue of mixing elsewhere. Although substantial work has been done since the publication on bottom boundary mixing by

Thorpe (1987), we may still quote him: "boundary layers on slopes have been given less attention than they deserve, particularly in view of their possible effects in [..] sediment stability and the production of nephel layers (Dickson and McCave, 1986), and their importance to benthic fauna". It is within this context that we will first discuss the occurrence of internal waves over the slope of the Faeroe-Shetland Channel, then the structure of nepheloid layers and the depths where erosion may be expected, and finally the cross-slope zonation of indicators for recent deposition in the sediment (e.g. organic carbon, phytopigments, ^{210}Pb).

2. Study area

The Faeroe-Shetland Channel (FSC, 60°N, 6°W–63°N, 1°W) is one of the major conduits of the global conveyor belt system as it connects surface waters of the North Atlantic with the Norwegian Basin as well as deep waters of the Norwegian Basin with the Iceland Basin. The West Shetland Shelf borders it in the southeast, where it connects the North Atlantic with the North Sea (Fig. 1). The northern entrance is 1500–2000 m deep; the southwestern connections have sills with maximum depths of about 850 m in the Faeroe Bank Channel and 600–650 m across the

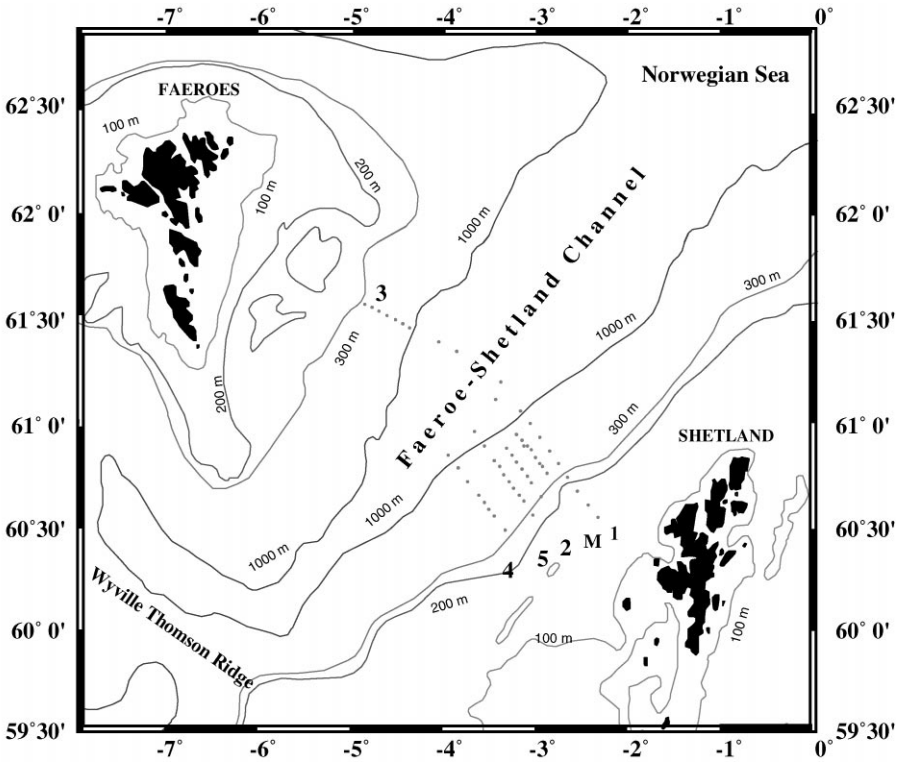

Fig. 1. Study area and sampling locations. Dots indicate stations along the hydrographic sections (#1, 2, 3, 4, 5; #M). For details on stations see Table 1.

Wyville–Thomson Ridge. The hydrography of the area was described extensively by Turrell et al. (1999). The upper 200–500 m of the water column is occupied by two distinct water masses of which North Atlantic Water (NAW) flows northward along the West Shetland Shelf break at a tidal mean speed of about $0.2\,m\,s^{-1}$ (Huthnance, 1986). Modified North Atlantic Water flows southward across the Faeroe Shelf and upper northwestern slope, turns in front of the Wyville–Thomson Ridge and then runs northward parallel to NAW along the central axis of the Channel. Water masses deeper than 500 m come in from the Norwegian Basin and flow southward towards the Wyville–Thomson Ridge (Turrell et al., 1999). The barotropic tide in the FSC is dominated by the semidiurnal M_2 that has an amplitude of 0.5–0.6 m in the FSC, runs parallel to the isobaths and has a phase difference of $\sim 20^\circ$ between the Wyville–Thomson Ridge and the northeastern entrance of the Channel (Sinha and Pingree, 1997). Maximum bottom current velocities as documented in Stoker et al. (1993) are $0.5–0.7\,m\,s^{-1}$ over the West Shetland Slope.

The shelf-break is positioned at about the 200-m depth contour (Stoker et al., 1993). The axis of the channel is at about 1200 m depth on our sections. Isobaths on the southeastern slope run parallel over long distances, and sediment types follow the depth contours. Biogenic carbonate contents are 20–80% on the West Shetland Shelf and $< 20\%$ below the shelf break. The sediments on the southeastern slope of the FSC consist of gravelly muddy sand between 200 and about 1000 m depth with patches of muddy sand, gravelly mud and sandy mud; deeper than 1000 m sandy mud dominates the sediment composition (Stoker et al., 1993).

We have selected this area for our research because the slopes of the FSC are relatively gentle and not intersected by canyons. Furthermore, the opposing sloping sides favor internal wave reflections. Practically, the size of the basin is such that it could be covered by a modest oceanographic expedition.

3. Materials and methods

3.1. Hydrographic sections

The sampling program ran from 30 April (day 120) to 17 May 1997 (day 137). Six CTD sections were occupied perpendicular to the axis of the channel, five across the southeastern slope at mutual distances of 5–10 nautical miles, and one across the northwestern slope (Fig. 1). The distances between the stations on the sections were 2.5, 5 and 10 nautical miles depending on vertical gradients and position on the slope. Here, we will focus on section #1 across the southeastern slope running from 60°33.07′N, 2°21.00′W at 149 m depth to 61°11.39′N, 3°23.34′W at 1213 m depth for hydrographic data, and section #M, running from 60°49.68′N, 3°00.48′W at 500 m depth to 61°10.00′N, 3°34.02′W at 1228 m depth on which, in addition to regular CTD casts, moorings were deployed and bottom samples were collected. Data from the other sections will be given only where they provide additional information.

3.2. Water column

The water column was sampled with a Seabird SBE-911 plus CTD equipped with a Sea-Tech transmissometer (660–670 nm, 0.25 m lightpath) and a 'Chelsea Instruments Aquatracka'

fluorometer (excitation wavelength 440 nm and bandwidth 80 nm, detection wavelength 670 nm and bandwidth 30 nm). The light attenuation coefficient c_0 (m^{-1}) was calculated from transmission as $c_0 = \ln(\text{transmission})/0.25$. The sensors on the CTD sampled at a frequency of 24 Hz, presented here as averages over 1-m depth intervals during the downcast.

Water samples were collected during upcasts with 12-l NOEX bottles at about every 100 m and at additional depths when the CTD downcast showed strong gradients. Surface samples refer to depths between 10 and 15 m, the deepest samples to 10–30 m above the bottom (mab). Entire NOEX bottles were emptied in carboys that were transported to the cooled van (4–6°C) on board of the ship for further processing. The carboys were shaken vigorously before subsampling, 2 l for total particulate matter (TPM), 2 l for particulate organic matter (POC, PON, $\delta^{13}C$), and 1 l for chlorophyll-*a* (chl-*a*). TPM was determined by low-vacuum filtration over pre-weighted Poretics polycarbonate membrane filters (47 mm diameter, 1 μm pore size), with rinsing of the filters with milliQ water to remove the salt, drying (60°C, 24 h), equilibration to 30% ($\pm$ 0.1%) relative humidity (RH), and re-weighing at 30% ($\pm$ 2%) RH. A pore size of 1 μm was chosen to stay as close as possible to the filters used for POC (see below) and to prevent overloading of the filters. In our experience and in literature data (Sheldon, 1972) the possible bias in TPM weight introduced by this pore size relative to the more usual 0.45 μm is small compared to other biases associated with the determination of TPM from bottle samples (Bishop, 1991). We included humidity control in the weighing procedure to exclude variability due to the uptake of water vapor from the laboratory atmosphere (40–80% RH), which would occur during transfer from the dessiccator to the balance and during weighing. Accuracy of the TPM weights is better than 0.04 mg at the 95% confidence level.

Samples for particulate organic matter were filtered over precombusted (480°C, 6 h) Gelman A/E borosilicate fibre filters (13 mm diameter, 1 μm nominal pore size). Particulate organic carbon (POC) and nitrogen (PON) of the material on the filters were measured with a Carlo-Erba NA 1500-2 elemental analyzer following the protocol of Verardo et al. (1990). Inorganic carbon was removed with sulfurous acid. Accuracy expressed as the coefficient of variation for replicate samples, was about 0.025 for POC and 0.07 for PON. Carbon isotope ratios of the organic matter collected on the filters were measured with a VG-optima SIMS coupled on-line via a continuous flow interface with the Carlo-Erba elemental analyzer. Results are reported in the δ notation relative to the Vienna-PDB. Reproducibility was better than 0.1‰.

Samples for chlorophyll-*a* (chl-*a*) were filtered over Whatmann GF/C borosilicate fiber filters (55 mm diameter, 1.2 μm nominal pore size) before fluorometric determination according to Holm-Hansen et al. (1965).

3.3. Currents

An upward looking 75 kHz narrow-band RDI-ADCP, equipped with a CTD unit, was moored at 595 m water depth on section # M (Fig. 1, Table 1). The instrument measured currents averaged over 4-m bins between 150 and 546 m depth, at time ensembles of 10 min from 3 May (day 123) to 16 May 1997 (day 136). Aanderaa RCM9, Valeport BFM308 and NBA-DNC 2M current meters were moored at 8 and 34 mab at two stations on section # M (Fig. 1, Table 1) during days 122–136. Accuracy of the current data based on 10-min ensembles is $\pm$ 1 cm s^{-1} and $\pm$ 5° for speed and direction. The horizontal Cartesian coordinates were rotated anticlockwise over 40° to match the

Table 1
Position, depth, sediment median grain size (surface 2.5 mm) with % of particles $< 60\,\mu m$ (in brackets) and % of inorganic C (IC) of the mooring and multi-corer stations. Particle size was not measured at St. 54 due to lack of sufficient sample material

Station	Latitude (N)	Longitude (W)	Depth (m)	Median grain size (μm)	Instruments in moorings/IC content (%)
Moorings					
26	60°49.65′	3°00.47′	502	—	Current meters
25	60°52.82′	3°04.40′	595	—	ADCP
27	60°55.48′	3°10.49′	708	—	Current meters
Multicorer stations					
38	60°54.22′	3°06.81′	649	274 (11%)	1.3
78	60°55.19′	3°08.22′	672	264 (11%)	1.4
23	60°55.76′	3°10.55′	711	210 (7%)	1.0
28	60°56.84′	3°12.56′	766	160 (10%)	1.0
56	60°57.33′	3°13.92′	801	158 (15%)	1.1
34	60°56.68′	3°16.79′	900	160 (15%)	1.2
66	60°59.17′	3°19.15′	978	195 (18%)	0.9
54	61°09.99′	3°33.95′	1228	Not measured	1.2

mean bathymetry. Thus, along-slope components (u) are positive to the northeast, and cross-slope components (v) are positive to the northwest (off-slope). All data were low-pass filtered with the cut-off frequency at 1 cph prior to further analysis.

3.4. Sediment

Sediment samples were collected with a multiple corer (Barnett et al., 1984) at eight stations on section #M (Fig. 1, Table 1). The corer was equipped with eight polycarbonate liners with inner diameter of 62 mm, which normally collected virtually undisturbed cores of 25–35 cm length with clear overlying water. Cores that were turbid or disturbed otherwise were discarded. Immediately after retrieval on deck, the cores were transported to the cooled van (4–6°C), where they were sectioned into slices of 2.5 mm in the upper 1 cm of the sediment, 5 mm from 1 to 3 cm, 10 mm from 3 to 7 cm, and 20 mm from 7 to 15 cm depth. The sediment slices of corresponding depth intervals from 3 to 4 cores were pooled and frozen (-80°C for pigments, -20°C otherwise) until further analysis. Water content was determined from the loss of weight after drying at 60°C for 48 h and correcting for the salt content of the interstitial water. Dry bulk density and porosity were calculated from the water content and the bulk weight of the samples, applying a density of $2.6\,g\,cm^{-3}$ for the dry solids. Grain size distributions (0–2.5 mm slices) were measured by sieving over 1 mm mesh and laser diffraction of the particles < 1 mm (Coulter LS 230) after removal of organic matter with 30% H_2O_2 at 40°C and carbonates with 0.5 N HCl at 80°C. The grain size distribution measured with the Coulter LS 230 was corrected for the weight retained on the 1 mm sieve. Carbon and nitrogen contents of the (not fractionated) dried and homogenized slices were determined on a Carlo-Erba NA-11500 elemental analyzer, according to Verardo et al. (1990).

Total carbon (TC) and total nitrogen (TN) were determined by the combustion of untreated samples in tin cups, total organic carbon (TOC) after the removal of inorganic carbon by the addition of small aliquots (10–50 μl) of sulfurous acid to the cups. Inorganic carbon (IC) representing carbonates was calculated as TC minus TOC. Carbon isotopes of TOC were measured similarly to those of POC outlined previously. The accuracy, expressed as coefficient of variation, was about 0.01 for TC and TOC, and better than 0.02 for TN. The sediments were analyzed for chl-*a* and phaeophorbide-*a* (ph-*a*), which we regard as tracers for phytodetritus (Stephens et al., 1997), by means of reverse-phase HPLC equipped with a photodiode array plus fluorescence detector as described by Tahey et al. (1994) and Duineveld et al. (1997). For analysis of ^{210}Pb activity, sediment samples were spiked with ^{208}Po and leached with HNO_3 and HF in a microwave oven for 3 h, followed by spontaneous electrochemical deposition of Po-isotopes onto silver in 0.5 N HCl at 80°C for 4 h. ^{210}Pb activity was measured by alpha-spectrometry of ^{210}Po on a Canberra A-600-23-AM instrument with passivated implanted planar silicon detectors. Counting time was 48 h, counting error 3–7%.

4. Results

4.1. Hydrography and currents

Vertical profiles of salinity and potential temperature above the slope confirm the hydrographic settings as described by Turrell et al. (1999). Salinity gradually decreased in the upper 400 m, sharply decreased to a minimum between 400 and 500 m and increased again in the deepest layers (Fig. 2). Potential temperature showed largely similar profiles, with the main thermocline between 400 and 600 m depth (Fig. 2). Near the bottom of stations 9 and 10, the water was colder than at

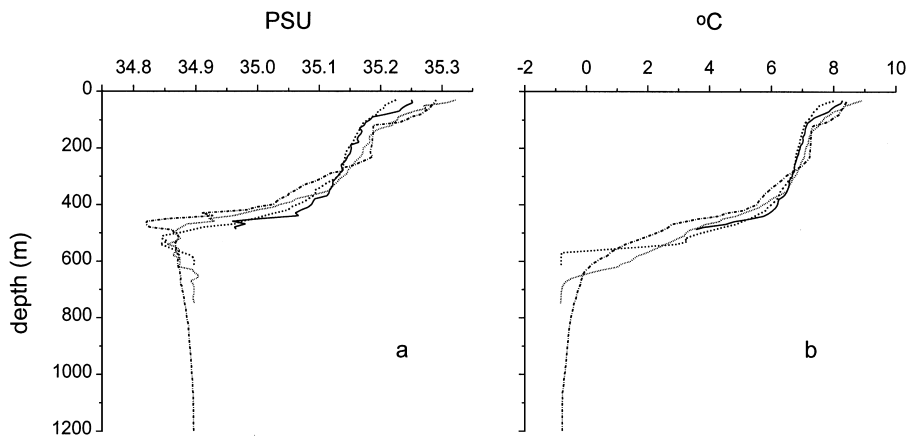

Fig. 2. Vertical profiles of (a) salinity and (b) potential temperature from stations 8 (solid line, 495 m), 9 (dashed line, 617 m), 10 (dotted line, 750 m) and 12 (dashed–dotted line, 1213 m). All stations lie on section #1; the profiles were measured on day 120.

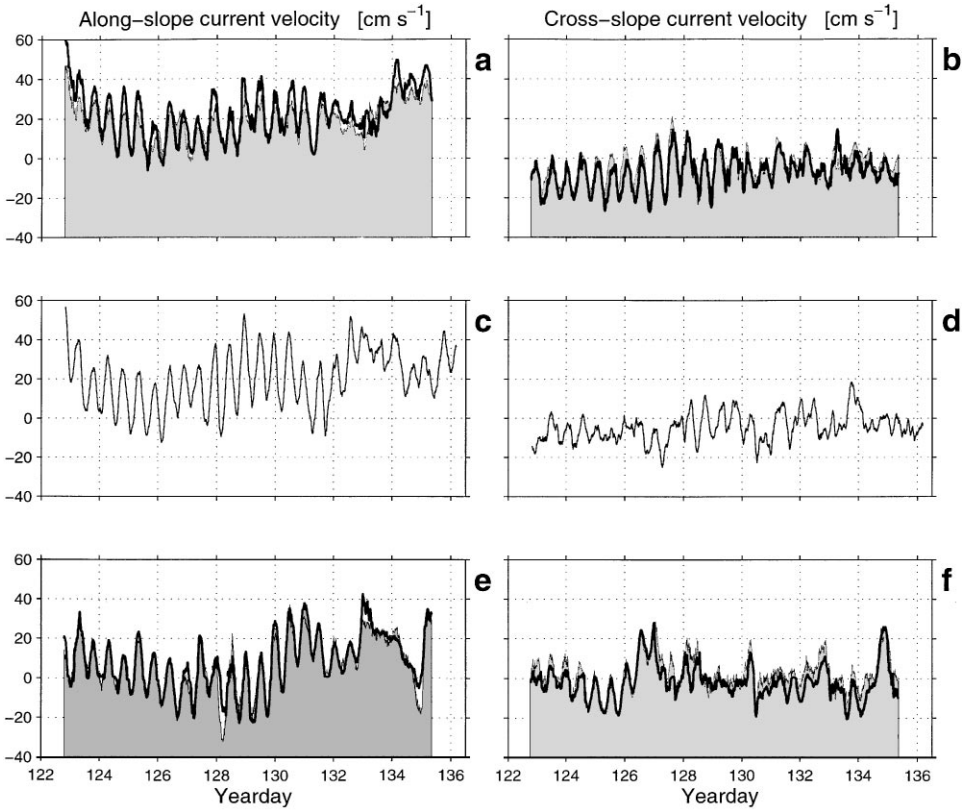

Fig. 3. Along- and cross-slope near-bottom currents at (a,b) St. 26 at 502 m, (c,d) St. 25 at 595 m, and (e,f) St. 27 at 708 m. Shaded background refers to measurements at 8 mab, solid lines to 34 mab (a,b,e,f) or 50 mab (c,d).

similar depths at deeper nearby stations, indicating that the pycnoclines were crawling up-slope around 600–800 m.

Average near-bottom along-slope currents (u) were directed northeast at mean velocities (34–50 mab) of 0.22 m s^{-1} at 502 m, 0.20 m s^{-1} at 595 m, and 0.08 m s^{-1} at 708 m (Fig. 3a, c, e). Mean values of u were 5–15% lower at 8 mab than at 34 mab. Variability around the mean was high as indicated by SDs of 0.12, 0.15 and 0.14 m s^{-1}, respectively, at 34–50 mab. Standard deviations of u were 5–20% lower at 8 mab than at 34 mab. Low-frequency along-slope currents alternated direction at the deepest stations, most notably at 708 m between days 126 and 130. Cross-slope mean currents (v) were up-slope at 34–50 mab at all three stations: -0.07 m s^{-1} at 502 m, -0.05 m s^{-1} at 595 m and -0.01 m s^{-1} at 708 m (Fig. 3b, d, f). At 8 mab, mean v was down-slope at 708 m (0.03 m s^{-1}) and up-slope at 502 m (–0.04 m s^{-1}), which is 40% less than at 34 mab. The SD of v was 0.07–0.09 m s^{-1} in all series, which is considerably lower than along slope, but large when compared to the mean v. At 708 m, periods with down-slope currents that lasted several hours appeared at both 8 and 34 mab about every second day after day 126. Associated with these periods, currents could change from $+0.2$ to -0.2 m s^{-1} within about 1 h (e.g. on day 130).

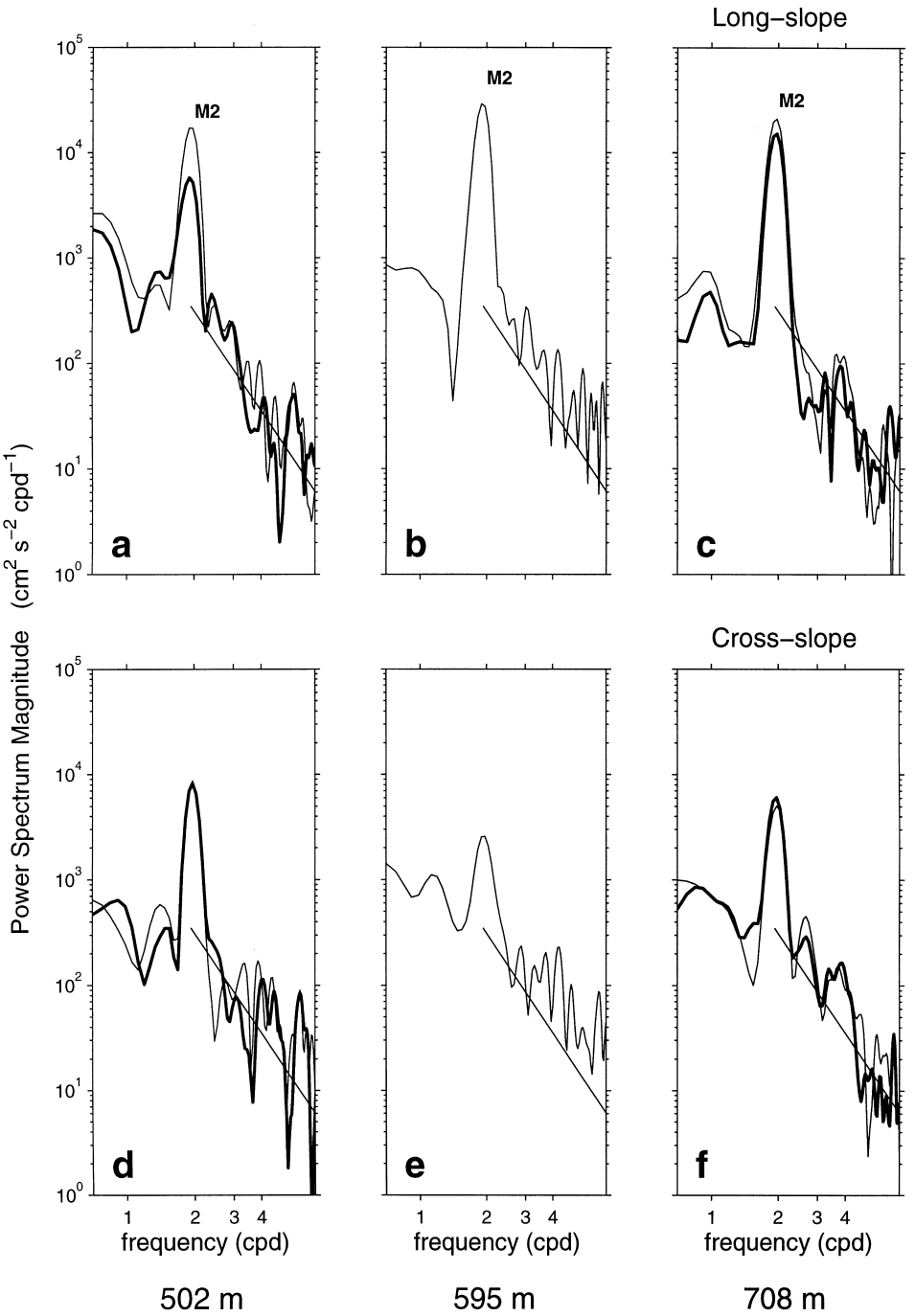

Fig. 4. Power spectra (Hanning window, equivalent with 19 degrees of freedom) of the along-slope (a,b,c) and cross-slope currents (d,e,f) observed at 34, 50 mab (thin lines) and 8 mab (thick lines) on the southeastern slope at 502 m (a,d), 595 m (b,e) and 708 m (c,f) total water depth. Thin lines with slope 2 : 1 indicate the predicted Garrtett–Munk spectra for internal waves. The inertial frequency f is at 1.75 cpd, M_2 at 1.93 cpd.

Variance in the *u, v* current components was predominantly semi-diurnal lunar tidal and was approximately in phase at the three stations. The spectra of the currents followed the Garrett–Munk prediction for internal waves (Fig. 4). Along slope, the M_2-peaks were uniformly high at all depths, although it was lower for 595 m, 8 mab. These results are in contrast to those of the cross-slope currents for which the M_2 peak was relatively small at 595 m, intermediate at 708 m and sharpest at 502 m. Notably, cross-slope M_2 was enhanced relative to along-slope M_2 in the 8-mab record of the 502-m station. This indicates that the kinetic energy in the M_2 band was predominantly in the along-slope current at 595 m, but that it was aligned towards the cross-slope current at 502 m, particularly near the bottom.

To further elaborate the *u, v* variability around the M_2 band we applied a Butterworth high-pass filter to the data with a cut-off frequency of $0.5\,d^{-1}$. From the filtered data we calculated the principal axes of current velocity using the formula outlined in Emery and Thomson (1998). We added series from the nine deepest bins of the ADCP at 595 m, thus covering the 50–82 mab range, to better identify changes with depth. Results show that the tidal variability was aligned almost along slope higher up in the water column, bending slightly and clockwise when approaching the bottom (Fig. 5). The main axis deviated $\sim 12^\circ$ from along slope at 34–50 mab at the 595 and 708-m stations, and $\sim 16^\circ$ at 8 mab. At 502 m, however, it deviated 40° at 34 mab and as much as 60° at 8 mab. The ratio of the axes of the ellipses decreased from 1.7 to 2.4 off the bottom to ~ 1.5 at 8 mab. These observations indicate that near-bottom currents in the semidiurnal band were aligned cross slope rather than along slope at, particularly, the 502-m station.

4.2. Chl-a and TPM distribution

TPM varied from 0.2 to $1.3\,g\,m^{-3}$ (average $0.57\,g\,m^{-3}$, SD $0.28\,g\,m^{-3}$) with nine out of 178 samples exceeding this range upto $2.4\,g\,m^{-3}$. Based on high *t*-values of their studentized residuals, referring TPM against beam attenuation c_0, these nine data points were considered as outliers and omitted in further analysis. An example of the vertical distribution of TPM in the water column (Fig. 6a) shows higher concentrations at mid-depth and close to the bottom. POC concentrations were highest in the upper 200 m of the water column (50–250 $mg\,m^{-3}$), corresponding to approximately 20% of TPM, and decreased towards the bottom (Fig. 6b). Near-bottom chl-*a* concentrations were two orders of magnitude lower than near the surface (Fig. 6c). The mid-depth peak of TPM was reflected in chl-a and in the relatively low POC/TN and high chl-*a*/POC ratios (Fig. 6d, e). The $\delta^{13}C$ ratio of POC varied between -23.5 and $-25.5‰$ without any trend with water depth or station, matching the range of values reported for POC in the mixed surface layer at about 60°N (e.g., Goericke and Fry, 1994).

4.3. Fluorescence and beam attenuation versus bottle samples

Fluorescence (flc) was highly correlated with extracted chl-*a* for chl-$a > 7\times10^{-6}\,g\,m^{-3}$ and flc > 0.02 (chl-$a = 3.36\times flc^{1.42}$, $R = 0.95$, $n = 54$). Light attenuation c_0 was not correlated to TPM when the entire data set was used ($R = 0.005$, $n = 169$, Fig. 7a), which may be due to the dominance of phytoplankton cells in samples from the surface layers. Plotting c_0 against fluorescence showed a strong correlation (Fig. 7b). We subtracted the contribution of chl-*a* from the attenuation signal to obtain the corrected attenuation: $c_{-flc} = c_0 - 0.61\times flc$, which appeared to be slightly better

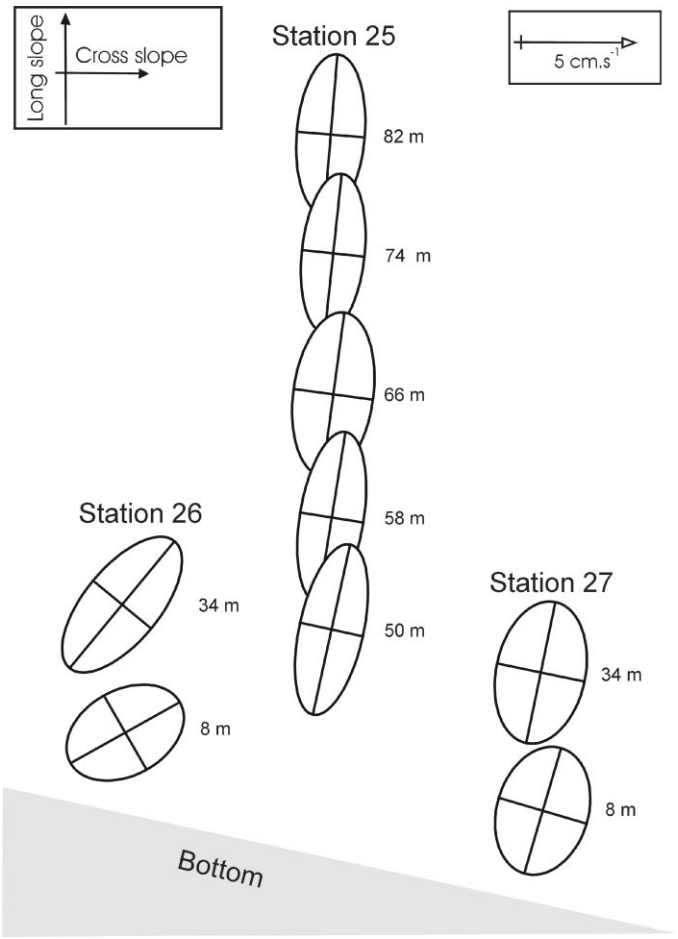

Fig. 5. Ellipses of the high-pass filtered current velocities (cut-off 0.5 cpd) at St. 26 (502 m), St. 25 (595 m) and St. 27 (708 m). The depth indicated with the ellipses is relative to the bottom. Lengths of the axes (for scale see legend in upper right corner) are computed to define the 95% confidence region for the velocity fluctuations.

correlated with TPM (Fig. 7c). The slope of TPM versus $c_{-\mathrm{flc}}$ is flat but within the range given by, e.g., Baker and Lavelle (1984) and Bishop (1986). Our TPM values span a range of about 1 g m^{-3} only, and scatter of this order of magnitude appears in most other field studies (e.g. Puig and Palanques, 1998). This is most likely due to bottle-to-bottle variability influencing filtered TPM values. In subsequent sections we will interpret the corrected attenuation $c_{-\mathrm{flc}}$ as a proxy for particulate matter concentrations.

4.4. Nepheloid structure

The stratification of the water column (Fig. 2) is reflected by high values of the buoyancy frequency (N), which we calculated for 10-m depth intervals and normalized over the inertial

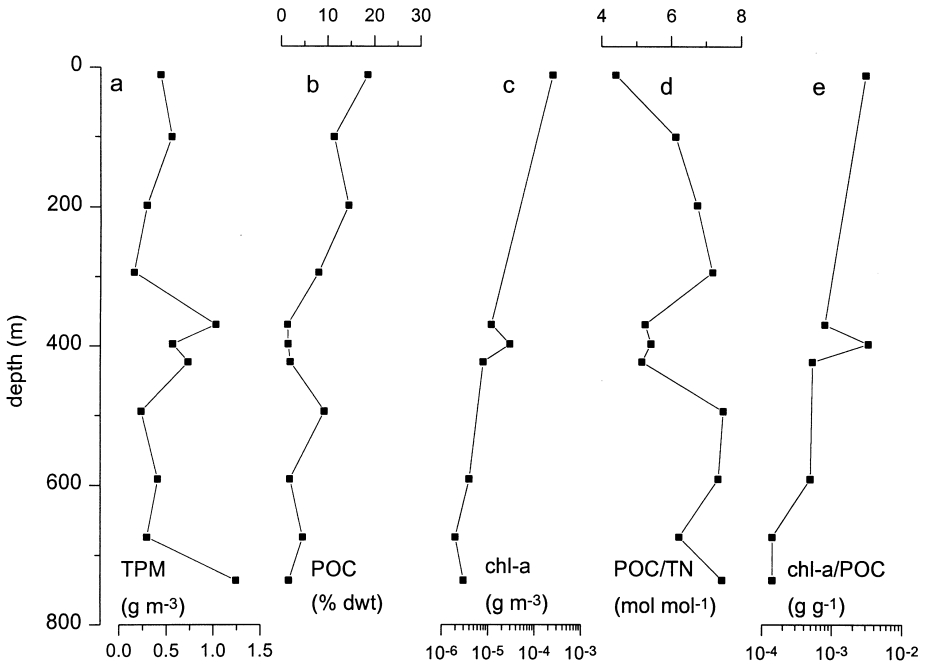

Fig. 6. Vertical profiles of (a) TPM, (b) POC as % of TPM, (c) chl-*a*, (d) POC/TN ratio of TPM, and (e) chl-*a*/POC ratio in bottle samples collected at St. 10 (750 m).

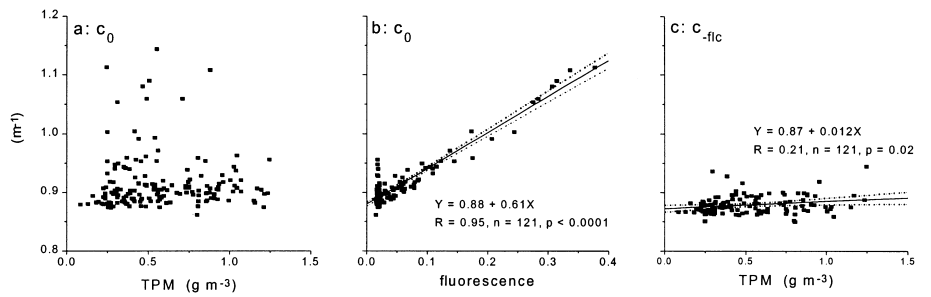

Fig. 7. Correlation diagrams between (a) TPM and beam attenuation c_0, (b) beam attenuation c_0 and fluorescence, and (c) TPM and the corrected (see text) beam attenuation $c_{-\mathrm{flc}}$.

frequency f, $1.27 \times 10^{-4}\,\mathrm{s}^{-1}$ at 61° north. Profiles show strong stratification with $N/f = 30$–50 in the surface 100 m, $N/f < 30$ between about 100 and 350 depth and a sharp increase at about 350–400 m to peak values of 50–90 at 500–600 m depth (Fig. 8a). Additional peaks of N/f as high as 40–50 were observed at 600–700 m in some, but not all, profiles. Deeper in the water column N/f rapidly decreased to values less than 10. Sub-surface peaks in fluorescence were situated directly above the depth where N/f strongly increased (Fig. 8c).

Increased turbidity associated with nepheloid layers generated on the slope was expected at critical frequencies for internal wave reflection. For geometric focusing of internal waves distinct

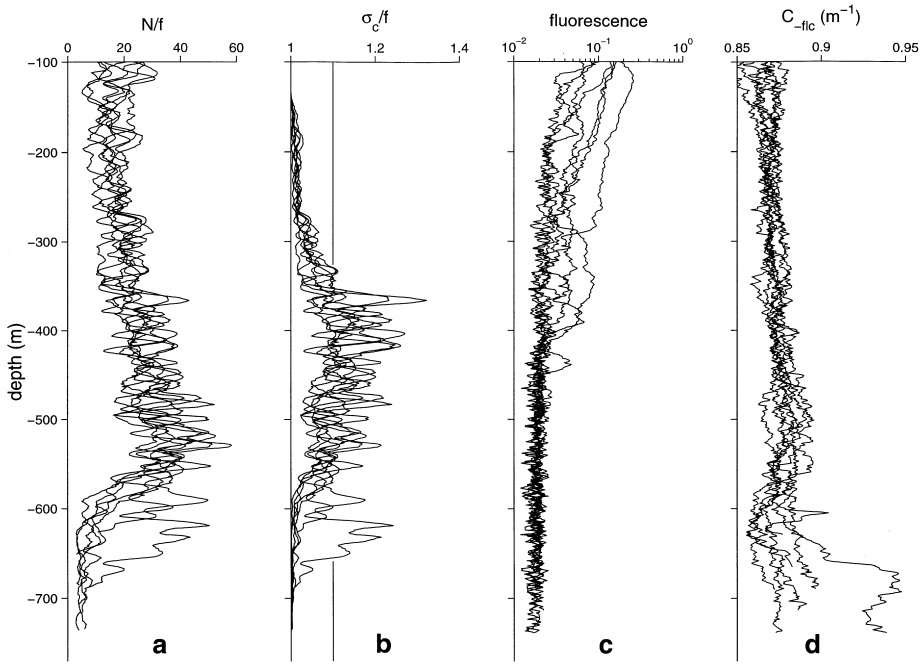

Fig. 8. Vertical profiles of (a) the buoyancy frequency N, (b) the critical internal wave frequency σ_c, both normalized over the inertial frequency f, (c) fluorescence and (d) corrected (see text) beam attenuation $c_{-\mathrm{flc}}$. Profiles are from all seven stations between 700 and 800 m depth on the southeastern slope of the channel (sections #1, 2, 4, 5, #M). Vertical line in (b) indicates the M_2 frequency normalized over f.

zones on the slope which allow for sub-critical and super-critical reflections should be present. The critical frequency (σ_c) is related to the gradient of the sea bed (α) by (Thorpe, 1987):

$$\sigma_c^2/f^2 = N^2/f^2 \sin^2\alpha + \cos^2\alpha. \quad (1)$$

We calculated α as a function of depth at 10-m intervals by averaging the gradients of all five sections on the southeastern slope of the channel and smoothing with a 50 m moving average to remove effects of local irregularities. The slope angle varied between 0.01 and 0.045 rad (0.6–2.6°), with maxima at about 400, 650 and 900 m, which causes the slight differences between the profiles of N^2/f^2 and σ_c^2/f^2 (Fig. 8b). On average, σ_c/f peaked at shallower depth than N/f, but both σ_c/f and N/f showed considerable variability around the mean pattern between 350 and 650 m with several maxima and minima in the individual profiles. The dominant tidal frequency M_2, ($M_2/f = 1.10$) may be critical ($M_2 = \sigma_c$) or sub-critical ($M_2 < \sigma_c$) at depths generally between about 350and 550 m (Fig. 8b). Turbidity as indicated by beam attenuation $c_{-\mathrm{flc}}$ gradually increased to maximum values at about 500–550 m, dropped to relatively low values around 600 m and increased again toward the bottom (Fig. 8d), thus suggesting the presence of benthic nepheloid layers (BNLs) extending ~ 100 mab.

Contour plots of N/f, σ_c/f and $c_{-\mathrm{flc}}$ were constructed for section #1 (Fig. 9). Stratification was generally strongest between 400 and 650 m depth over the entire southwestern slope, but it peaked

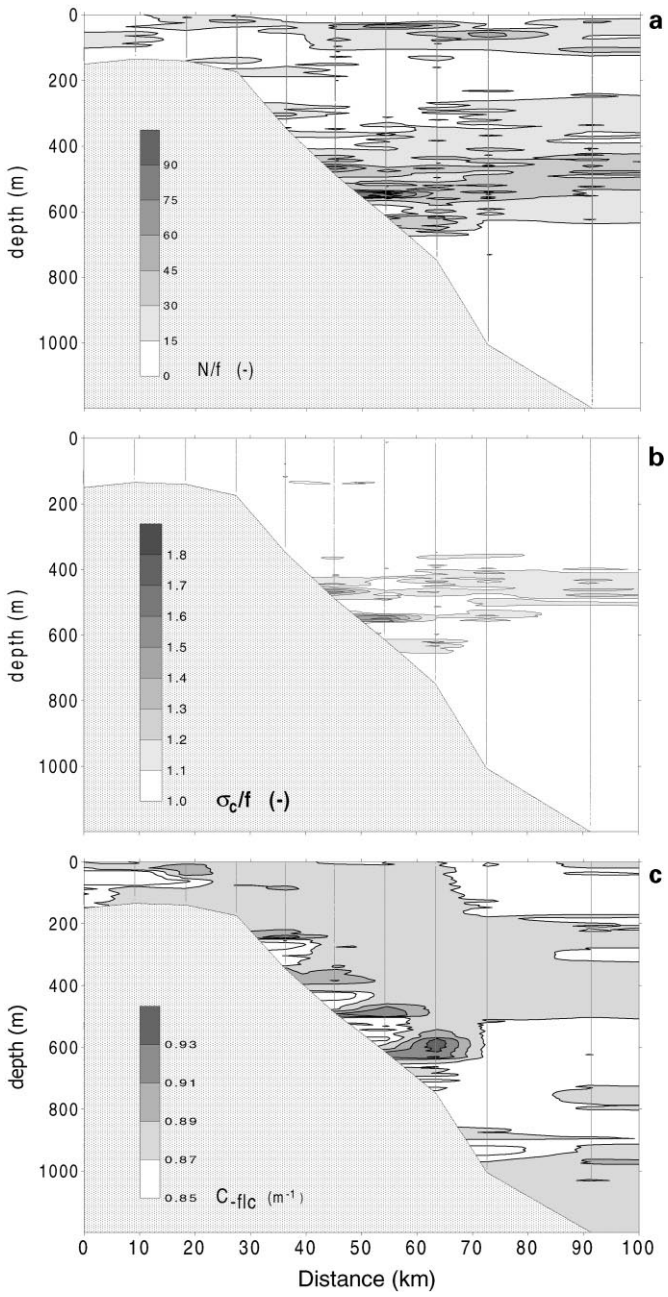

Fig. 9. Contour plots of (a) normalized buoyancy frequency N/f, (b) normalized critical frequency σ_c/f, and (c) corrected (see text) beam attenuation c_{flc}. In (b) scaling is chosen such that contours are filled with grey to black where $\sigma_c > M_2$. Data were collected on section #1, vertical lines indicate CTD stations. Horizontal axis is in km relative to the start of the section at 60°33.07′N, 2°21.00′W. The West Shetland Shelf is to the left.

close to the slope at 500–600 m (Fig. 9a). This pattern was reflected in the distribution of the critical frequency σ_c/f, which was larger than M_2/f close to the bottom in three layers between 450 and 650 m (Fig. 9b). Beam attenuation was moderately enhanced in a thick BNL extending from the shelf break to the major density gradient at 400–600, where it formed a weak INL along the pycnoclines (Fig. 9c). Erosion and BNL-INL formation was indicated between 450 and 650 m depth, corresponding to the zones where reflection of the semi-diurnal tidal waves is critical.

4.5. Sediment data

Sediment samples could be taken at stations deeper than about 600 m only. Sediments between 300 and 450 m consisted of hard sands, which our corer could not penetrate, and between 450 and 600 m the sea floor was densely covered with gravels and cobbles deposited during the last glacial ice retreat. Median grain size decreased from 274 μm at 649 m to 158 μm at 801 m, and the clay/silt fraction (< 60 μm) varied between 7 and 18% (Table 1). Sediments were low in carbonates (inorganic carbon $\approx 1\%$, Table 1) over the entire transect. Total organic carbon (TOC) contents of the sediments at stations deeper than 600 m were low, between 0.15 and 0.6%, without consistent trends, either with depth in the sediment or with water depth (Table 2). The average atomic TOC/TN ratio of the samples was 8.3 with slightly lower ratios at the sediment–water interface than deeper in the sediment (Table 2). A relatively low TOC/TN ratio of 6.6 was measured in the upper 5 mm at 672 m water depth. The $\delta^{13}C$ value of the organic matter was $-21.9‰$ at 672 and

Table 2
Total organic carbon (TOC), TOC to total nitrogen ratio (TOC/TN), chlorophyll-*a* (chl-*a*), phaeophorbide-*a* (ph-*a*) and $\delta^{13}C$ of the TOC in the top-layer (0–5 mm) and the 5–80 mm layer of sediments at the slope of the Faeroe-Shetland Channel. Numbers in parentheses are 1 SD and indicate variability with depth within the layers (0–5 mm, $n = 2$ sub-layers; 5–80 mm, $n = 10$ sub-layers). Data for chl-*a* and ph-*a* refer to 0–5 and 5–30 mm depth

Station-depth (m)	Layer (mm)	TOC (%)	TOC/TN (mol mol^{-1})	$\delta^{13}C$ (‰)	Chl-*a* (ng g^{-1})	Ph-*a* (ng g^{-1})
38–649	0–5	0.25 (0.02)	7.9 (0.1)	−23.4 (1.2)	38 (5)	713 (55)
	5–80	0.26 (0.04)	8.3 (0.4)		11 (3)	321 (202)
78–672	0–5	0.30 (0.04)	6.6 (0.6)	−21.9 (1.0)	18 (8)	601 (3)
	5–80	0.25 (0.05)	7.5 (0.9)		17 (2)	481 (110)
23–711	0–5	0.22 (0.05)	7.7 (1.6)	−21.9 (0.2)	—	—
	5–80	0.24 (0.04)	8.3 (0.3)	—		
28–766	0–5	0.23 (0.02)	8.4 (1.9)	−24.2 (1.0)	38 (20)	863 (350)
	5-80	0.24 (0.04)	8.2 (0.9)	—	12 (7)	458 (100)
56–801	0–5	0.23 (0.01)	7.7 (0.3)	−23.2 (0.6)	29 (22)	779 (118)
	5–80	0.27 (0.04)	8.6 (0.5)	—	7 (1)	479 (21)
34–900	0–5	0.23 (0.01)	8.1 (0.1)	−25.1(0.4)	69 (21)	984 (48)
	5–80	0.28 (0.05)	7.8 (0.9)	—	14 (5)	653 (46)
66–978	0–5	0.27 (0.01)	7.9 (0.9)	−23.1 (0.1)	72 (23)	1149 (107)
	5–80	0.25 (0.05)	7.8 (0.6)	—	14 (10)	687 (250)
54–1228	0–5	0.30 (0.01)	8.7 (0.2)	−24.4 (0.6)	28 (13)	420 (100)
	5–80	—	—	—	7 (13)	304 (45)

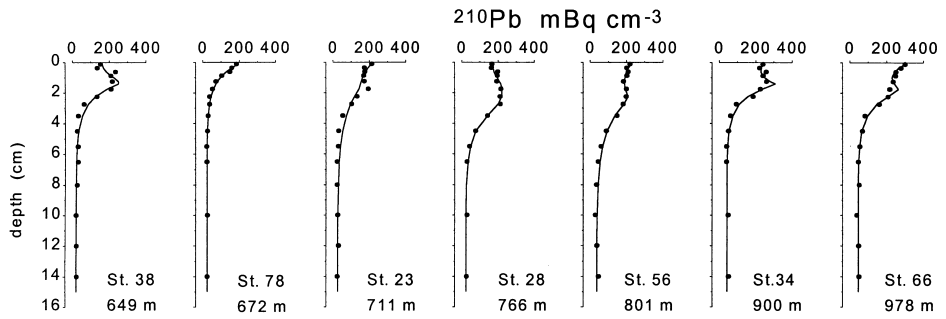

Fig. 10. Vertical profiles of ^{210}Pb activity along section #M. Activities were measured as Bq kg^{-1} dry sediment and converted to mBq cm^{-3} wet sediment volume using data on dry bulk density of the sediment samples. Symbols are measured data; lines are best fits of the models described by Soetaert et al. (1996) neglecting sediment accumulation.

711 m depth and -23.1 to -25.1‰ at the other stations (Table 2), close to the values measured in POC in the water column. Concentrations of chl-*a*, indicative of labile phytodetritus, were highest in the upper 5 mm of the sediments, especially at the deeper stations on the slope (Table 2). Lowest concentration in the 5 mm surface layer was measured at 672 m, 18 ng g^{-1}, compared to 29–72 ng g^{-1} at the other stations. Below 5 mm variability between stations was much less with concentrations between 7 and 17 ng g^{-1}. The data for phaeophorbide-*a* (ph-*a*), which is a degradation product of chl-*a*, showed a similar pattern with higher concentrations in the top layers compared to the layers below, and a relatively low concentration in the upper 5 mm at 672 m (Table 2). In all sediments, ph-*a* was more than an order of magnitude higher than chl-*a*, which indicates that degradation products dominate the phytopigment pool in these sediments.

^{210}Pb profiles were measured at seven stations between 649 and 978 m depth (Fig. 10). All profiles show excess ^{210}Pb concentrations in about the upper 6 cm relative to the background ^{226}Ra supported concentrations (about 20 mBq cm^{-3} at 649 m increasing to about 50 mBq cm^{-3} at 978 m). We applied the models of Soetaert et al. (1996) to determine the ^{210}Pb fluxes to the sediments. These models require estimates of the sediment accumulation rates as input. We assumed a range of this input parameter. Neglecting the accumulation rate relative to the rate of mixing assessed the lower limit, while the upper limit (varying from 0.1 mm yr^{-1} at 672 m to 0.3 mm yr^{-1} at 766–801 m) was estimated from the exponential decrease of the excess ^{210}Pb activity below the subsurface peaks. Because the fluxes should equal the ^{210}Pb inventories multiplied by the decay rate of ^{210}Pb ($\lambda = 0.0311$ yr^{-1}), the results were not very sensitive to the assumed range of sediment accumulation rates as long as the model outcomes matched the data.

Best fits through the measured data (Fig. 10) were obtained with models including non-local mixing (models 3 and 4a in Soetaert et al., 1996). This suggests that part of the ^{210}Pb bearing particles is injected, presumably by benthic fauna at 1–2 cm below the sediment–water interface, in addition to sedimentation on the sediment surface. Calculated ^{210}Pb total input fluxes vary from 60 to 250 Bq m^{-2} yr^{-1} with a distinct minimum at 672 m depth and highest fluxes at 766–801 m (Fig. 11). The contribution of the non-locally injected flux to the total input flux decreased with increasing water depth from about 90% at 649 m to about 55% at 978 m with a clear minimum of less than 30% at 672–711 m depth (Fig. 11). In fact, adding non-local mixing to the model did not

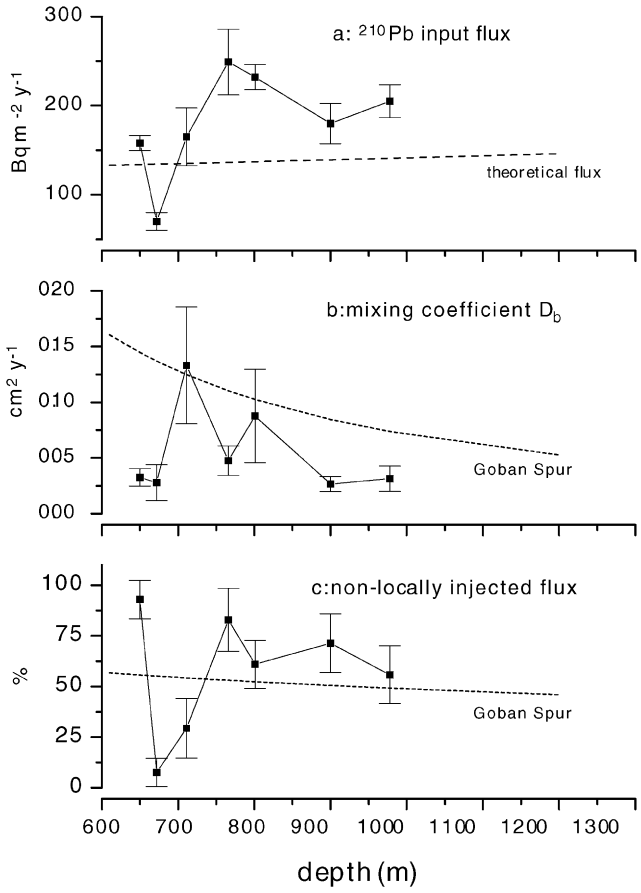

Fig. 11. (a) ^{210}Pb input flux, (b) mixing coefficient D_b, and (c) the contribution of the non-locally injected flux to the total input flux as derived from evaluating the data in Fig. 10 with the models of Soetaert et al. (1996). Error bars indicate $2 \times$ SD. The theoretical ^{210}Pb flux expected from atmospheric deposition and production from ^{226}Ra decay in the water column is indicated in (a). In (b) and (c) the general decrease with depth of both D_b and the contribution of the non-locally injected flux as computed by Soetaert et al. (1996) for Goban Spur (NW European margin, 47–50°N) is indicated for comparison.

improve the fit for the 672-m station. Model-derived mixing coefficients D_b were low (about $0.03\,cm^2\,yr^{-1}$) at the two shallowest stations, increased sharply to $0.13\,cm^2\,yr^{-1}$ at 711 m depth and subsequently decreased to $0.03\,cm^2\,yr^{-1}$ at stations deeper than 900 m (Fig. 11).

5. Discussion

In this study we aimed at identifying zonation of erosion–deposition processes on the slope of the FSC. Large along-slope transports through the FSC of different water masses in opposite directions (Van Aken, 1988; Turrell et al., 1999) and partly forming eddies and meanders (Van Aken,

1988; Oey, 1998; Burrows et al., 1999) ensure that observations made at different stations on our parallel cross-slope sections are not always directly coupled. Thus, increased turbidity at some depth is likely entrained somewhere upstream (e.g., Dickson and McCave, 1986; Puig and Palanques, 1998; Durrieu de Madron et al., 1999a). However, isobaths run parallel over long distances in the FSC, and canyons are absent. CTD surveys on sections up to 30 nautical miles towards the southwest showed basically similar profiles as on sections #1 and #M (Fig. 8). Also, the large-scale density distribution given by Turrell et al. (1999), which is based on sections further to the southwest and to the northeast, is almost identical to what we observed. Therefore, we are confident that our observations are representative for a wider area and that for the present purpose 2-D interpretation of the data is allowed.

5.1. Internal waves impinging on the slope

On scales much longer than tidal, surface water flows northward along the West Shetland Shelf and water masses below ~ 600 m flow southward (see Turrell et al., 1999). On the basis of Ekman dynamics, Van Aken and Eisma (1987) suggested that these along-slope currents would induce up- and down-slope currents over the bottom and an intrusive flow to the interior of the channel where they converge. Our current meter data (Fig. 3) did not confirm this pattern. Instead, mean near-bottom along-slope currents were directed to the northeast between 502 and 708 m during the 2 weeks of observations, though the mean current at 708 m was $\sim 60\%$ smaller than at 595 and 502 m. Mean cross-slope currents were weak and up-slope, except for 8 mab at 708 m, which is opposite to what would be expected on the basis of Ekman dynamics. Apparently, other processes dominate the near-bottom current structure, and the relatively large tidal variability of the cross-slope currents (Figs. 3 and 4) suggests that internal tidal waves are important.

Temperature and density profiles at CTD stations that were repeatedly visited showed that the pycnoclines moved up and down over ~ 100 m. This may, however, be related to meanders of the boundary current, which are generated downstream of the Wyville–Thomson Ridge and have periods of 5–10 days (Oey, 1998). Meanders might be the cause of the rapid changes in the cross-slope currents measured at 708 m, although the period of these changes (about 2 days) is shorter than that given by Oey (1998). However, we would expect similar changes at the other stations and in the along-slope current velocity also. Alternatively, the rapidly changing near bottom cross-slope currents may indicate breaking waves or bores induced by the reflection of internal waves higher up the slope (De Silva et al., 1997).

Sherwin (1991) gave evidence for deep internal tides in the FSC. He showed that internal waves with M_2 frequency are generated at the Wyville–Thomson Ridge and propagate northward into the channel, where they may cause a flux of baroclinic tidal energy onto the slope, e.g. due to up-slope refraction. Internal tidal waves are generated throughout the basin when vertical displacements occur across the slope associated with the cross-slope component of the barotropic tide. Internal waves are generated most likely at topographic changes such as the shelf break. Enhancement of internal tidal energy is favored when the angle of the bottom slope exceeds that of the characteristic wave rays somewhere on the slope. As a result, internal waves would be concentrated where the tide has critical frequency (Huthnance, 1995), which in the FSC is mostly between 350 and 550 m depth (Fig. 8b) but may extend to as deep as ~ 650 m in discrete layers (Figs. 8b and 9b).

Application of a model based on linear internal wave theory (Gerkema, 1996) and considering the FSC geometry and average stratification suggested that internal waves in the M_2 band generated at the northwestern shelf break opposite to our sections follow a path that ultimately leads to reflection at 400–500 m depth on the southeastern slope (T. Gerkema, NIOZ, pers. comm.). This is exactly where the slope is critical for M_2, thus leading to enhanced internal tidal energy at that depth.

Detailed observations of internal wave reflections on sloping topography have indicated spectral enhancement and cross-slope alignment of current ellipses in a band around the critical frequency (Eriksen, 1998). Our data indicate cross-slope enhancement of M_2 at 502 m, particularly near bottom, possible enhancement at 708 m, but not at 595 m. This may be related to the discrete layering of the zones where M_2 frequency is critical. At 502-m water depth, near-bottom M_2-dominated current ellipses were aligned cross-slope rather than along-slope (Fig. 6), thus strongly indicating critical reflection of the semidiurnal tide at this depth.

5.2. Generation and sources of nepheloid layers

Resuspension is a prerequisite for nepheloid layers to develop, and mid-slope maxima of TPM are most likely related to localized erosion of the BNL and the seabed (Amin and Huthnance, 1999). Sources of TPM that fuel the upper slope may be the adjacent shelf and shelf break (Biscaye and Anderson, 1994; Brunner and Biscaye, 1997; Van Weering et al., 1998; Antia et al., 1999), settling from the productive surface layers (Biscaye and Anderson, 1994), and up-stream mud-patches (Durrieu de Madron et al., 1999a). In the FSC, sediment types follow the depth contours in the FSC (Stoker et al., 1993), and obvious source areas such as large mud-patches, either on the adjacent shelf or upstream, are absent. However, land masses are nearby, and the strong contour current with large-scale eddies and cross-slope meandering (Oey, 1998; Burrows et al., 1999) may carry sufficient amounts of particles from the shelf, the Wyville–Thomson Ridge or even further upstream. At the same time, this current may inhibit deposition near the shelf-break and on the upper slope (Stoker et al., 1991) and thereby provide the appropriate condition for gradual down-slope transport in a benthic nepheloid layer. A similar importance of the contour current for the resuspension and transport of TPM was identified in other studies (Courp and Monaco, 1990; Biscaye and Anderson, 1994; Puig and Palangues, 1998; Durrieu de Madron, 1999a, b; Van Weering et al., 1998).

The enhanced chl-*a* concentrations at mid-depth together with the low POC/TN and high chl-*a*/POC ratios in TPM, approaching those at the surface (Fig. 4), suggest that these particles originate from near the surface and not from the bottom. MacIntyre et al. (1995) showed that aggregated particles may accumulate from above at steep density gradients, and chl-*a* has been demonstrated to be an important constituent of such marine aggregates (e.g. Holloway and Cowen, 1997). However, 'fresh' algal debris cannot explain the observed $\sim 2.5\%$ POC content of the particles at mid-depth and thus suggests another origin. The large sand fraction in the sediment matrix provides a high background of organically poor material that is not readily resuspended. Normalizing TOC on the clay/silt fraction in the sediment that may be resuspended, here taken as $< 60\,\mu m$ (Table 1), gives TOC contents of 1.5–3%, which is very close to the POC content of TPM at mid-depth and in the bottom water. This, as well as the similar TOC/TN ratios and $\delta^{13}C$ of the organic matter in the surface sediment and near-bottom TPM, indicates that most of the

TPM in the bottom and intermediate nepheloid layers comes from the material on the slope and not directly from the surface.

The broad zone with weakly enhanced attenuation centered around 500–550 m in the $c_{-\mathrm{flc}}$ profiles and the pronounced increases towards the bottom (Fig. 9c, d) are a further indication of nepheloid layers fuelled by resuspension. Since transmissometers are most sensitive to small particles (Baker and Lavelle, 1984; Bunt et al., 1999), these signals may be caused by variability of the particle-size spectra with depth. However, observations with cameras in similar environments have indicated that large aggregates ($> 100\,\mu\mathrm{m}$) dominate the particle-size spectrum near the bottom (Thomsen and Van Weering, 1998), in which case the turbidity signal would indeed indicate strongly enhanced TPM concentrations. The shear leading to resuspension and detachment of the slope, forming the observed INL, may have disintegrated aggregates to smaller particles that could readily be sensed by transmissometers, thus causing additional increase in the $c_{-\mathrm{flc}}$ signal (Bunt et al., 1999).

The highest values of $c_{-\mathrm{flc}}$ were observed near the bottom, where the M_2 internal tide reaches critical and sub-critical angles. Our observations strongly suggest erosion and detachment of benthic nepheloid layers induced by critically reflecting waves. The main difference with the situation at Porcupine Bank described by Thorpe and White (1988) is that in the FSC it was not a change of slope angle that provided the conditions favorable for critical reflection, but the steep increase in the density gradient at mid-depth. Dickson and McCave (1986) also associated critical reflection with steep density gradients. However, in their situation northerly winds were necessary to sustain the suitable near-bottom stratification, thus causing nepheloid layers to occur intermittently. In the FSC strong stratification is persistent (Turrell et al., 1999) implying that the generation of intermediate nepheloid layers is likely to be a continuous feature.

5.3. Enhanced deposition deeper than 600 m

On the basis of the strong currents (Fig. 3) we expect minor deposition at the upper slope and erosion where the major pycnocline meets the bottom and internal tides are active. At the lower part of the slope current strength is reduced and deposition may be possible. Sediment focusing would cause most of the particles to be deposited in the deepest part of the channel, but rapid deposition from the INLs may retain the particles relatively high up the slope. Some box-cores were taken to collect macrofauna across the slope between 250 and 1250 m during the cruise. Hard sands with low fauna abundance were sampled between 300 and 450 m and sediments densely covered with large gravels between 450 and 600 m. The box-cores showed a 3–5 fold increase in the abundance of living species of deposit feeding bivalves and polychaetes at 500–600 m with maximum abundances between 650 and 800 m (R. Daan, NIOZ, pers. comm.). All this points to enhanced deposition deeper than about 600 m, though the FSC cannot be regarded as a major depocentre sensu Walsh et al. (1988) and Biscaye et al. (1994) for large parts of the adjacent shelf.

Chl-*a*:TOC ratios in the surface sediment (Fig. 12) are at least one order of magnitude smaller than in the bottom water, which implies that the phytoplankton material is either not deposited, which is unlikely given the ph-*a* contents of the sediment, or that it is retained in the sediment sufficiently long to have chl-*a* being decomposed, given a typical half-life time of days to weeks (Stephens et al., 1997). Rapid decomposition leaving highly aged materials in the surface sediment is confirmed by the low chl-*a*:ph-*a* ratios of $0.03–0.05\,\mathrm{g\,g^{-1}}$ shallower than 800 m and $0.06–0.07\,\mathrm{g\,g^{-1}}$ deeper down the slope.

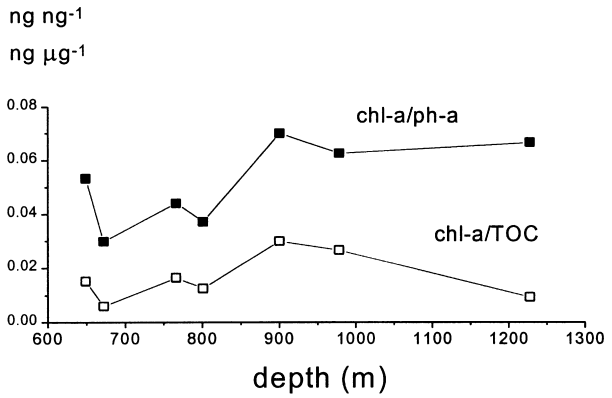

Fig. 12. Ratios of the pigments chlorophyll-*a* to phaeophorbide-*a* (chl-*a*/ph-*a*) and chl-*a* to total organic carbon (chl-*a*/TOC) in the 0–5 mm sediment surface layer as function of water depth along section ≠M.

A suitable indicator for particle transport and deposition is provided by ^{210}Pb inventories in the sediment with the theoretical input flux consisting of atmospheric deposition and ^{210}Pb production from ^{226}Ra decay in the water column (Cochran, 1982; Buesseler et al., 1985/1986; Bacon et al., 1994). Atmospheric deposition was set at 120 Bq m^{-2} yr^{-1}, using rates measured at our institute by Beks et al. (1998) and assuming an annual precipitation of 1000 mm. This flux is well in the range of values measured in the northern UK (110 ± 40 Bq m^{-2} yr^{-1}, listed in Thomson et al. (1993)). Water column production of ^{210}Pb was calculated from the difference between the concentrations of ^{226}Ra (1.63 Bq m^{-3}, based on GEOSECS St. 19 in the Norwegian Sea) and total ^{210}Pb (0.95 Bq m^{-3}, based on unpublished data of J.P. Beks, NIOZ, for two stations south of the Shetland Islands). With these assumptions we calculated an in situ contribution to the theoretical flux of 2.1 Bq m^{-2} yr^{-1} for every 100 m of water column, which is close to the ^{210}Pb-deficit of 2.4 Bq m^{-2} yr^{-1} per 100 m measured by Thomson et al. (1993) in the northeast Atlantic. At all stations, particularly those deeper than 750 m, the ^{210}Pb input fluxes estimated from the sediment profiles were larger than the sum of atmospheric deposition and decay of ^{226}Ra in the water column, thus indicating additional deposition of ^{210}Pb activity derived from lateral inputs. At St. 78 at 672 m depth, however, the ^{210}Pb input flux was distinctly less than expected theoretically, thus pointing to local erosion possibly associated with the maximum in turbidity at about this depth (Fig. 9).

We cannot exclude any contribution to the enhanced ^{210}Pb inventories from transports along the contours of the slope. However, a source localized higher up the slope or on the shelf is consistent with the beam attenuation profiles, and we expect that the INLs generated at mid-depth are efficient scavengers of ^{210}Pb. Furthermore, along-slope advected particles would most likely have their origin also on the slope or on the shelf, albeit upstream. The inventory of ^{210}Pb at St. 78 at 672 m is about 50% of the amount indicated by the theoretical influx. If we assume a similar 50% reduction of the inventory between 300 and 600 m and redistribute the excess rain of ^{210}Pb activity to the slope area between 700 and 1000 m, we would find an average ^{210}Pb input flux of about 200 Bq m^{-2} yr^{-1}. This is very close to what we measured. Thus, the observed pattern of ^{210}Pb

input fluxes deeper than 600 m is consistent with the off-slope input of particles from areas shallower than 600 m in addition to vertical settling fluxes.

We compared the estimated non-local injection and diffusive mixing rates of ^{210}Pb with the depth relationships as derived by Soetaert et al. (1996) for the Goban Spur continental slope (dashed lines in Fig. 11b, c). Clearly, mixing rates are relatively low, also when compared to the data compiled by Boudreau (1994), which for ^{210}Pb group around 0.1–0.5 $cm^2\,yr^{-1}$ at accumulation rates between 10^{-3} and 10^{-2} $cm\,yr^{-1}$. In contrast, the contribution of the non-locally injected flux to the total ^{210}Pb input is relatively large at most of our stations. Only at the 672 m deep station is faunal injection virtually absent. We suspect non-local mixing at 711 m to be underestimated, because the model fit completely missed the subsurface peak in the ^{210}Pb profile at this station. Apparently, it is the benthic fauna that by non-local mixing facilitates particle trapping to the sediments deeper than 600 m.

6. Conclusions

The major conclusions from our observations are: (1) Resuspension of bottom materials due to strong boundary currents mediates the formation of a benthic nepheloid layer at the upper slope of the FSC (shallower than $\sim$ 500 m). (2) Critical reflection of the semidiurnal internal tide at mid-depth ($\sim$ 500 m) causes erosion and detachment of the BNL, thereby generating an intermediate nepheloid layer that intrudes into the Channel. (3) Inventories of ^{210}Pb in sediments deeper than 600 m exceed atmospheric input plus water column production, indicating that materials transported within the nepheloid layers are being deposited at the lower slope of the Channel.

Acknowledgements

This work was financed by NIOZ as a pilot project for future studies in the FSC. The assistance and cooperation of technicians and crew of R/V *Pelagia* were of great help. We thank Harry Witte and Eilke Berghuis, who performed the pigment analysis, and Rogier Daan for putting his fauna data at our disposal. Theo Gerkema provided us with his latest modelling results. This is NIOZ contribution No. 3400.

References

Atzetsu-Scott, K., Johnson, B.D., Petrie, B., 1995. An intermittent, intermediate nepheloid layer in Emerald Basin, Scotian Shelf. Continental Shelf Research 15, 281–293.

Amin, M., Huthnance, J.M., 1999. The pattern of cross-slope depositional fluxes. Deep-Sea Research I 46, 1565–1591.

Antia, A.N., Von Bodungen, B., Peinert, R., 1999. Particle flux across the mid-European continental margin. Deep-Sea Research I 46, 1999–2024.

Bacon, M.P., Belastock, R.A., Bothner, M.H., 1994. ^{210}Pb balance and implications for particle transport on the continental shelf, U.S. Middle Atlantic Bight. Deep-Sea Research II 41, 511–535.

Baker, E.T., Lavelle, J.W., 1984. The effect of particle size on the light attenuation coefficient of natural suspensions. Journal of Geophysical Research 89, 8197–8203.

Barnett, P.R., Watson, O.J., Conelly, D., 1984. A multiple corer for taking virtually undisturbed samples from shelf, bathyal and abyssal sediments. Oceanologica Acta 7, 399–408.

Beks, J.P., Eisma, D., Van Der Plicht, J., 1998. A record of atmospheric ^{210}Pb deposition in the Netherlands. The Science of the Total Environment 222, 35–44.

Biscaye, P.E., Anderson, R.F., 1994. Fluxes of particulate matter on the slope of the southern Middle Atlantic Bight: SEEP-II. Deep-Sea Research II 41, 459–509.

Biscaye, P.E., Flagg, C.N., Falkowski, P.G., 1994. The Shelf Edge Exchange Processes experiment, SEEP-II: an introduction to hypotheses, results and conclusions. Deep-Sea Research II 41, 231–252.

Bishop, J.K.B., 1986. The correction and suspended particulate matter calibration of Sea Tech transmissometer data. Deep-Sea Research 33, 121–134.

Bishop, J.K.B., 1991. Getting good weight. In: Hurd, D.C., Spencer, D.W. (Eds.), Marine Particles: Analysis and Characterization. Geophysical monographs 63, A.G.U., pp. 229–234.

Boudreau, B.P., 1994. Is burial velocity a master parameter for bioturbation? Geochimica et Cosmochimica Acta 58, 1243–1249.

Brunner, C.A., Biscaye, P.E., 1997. Storm-driven transport of foraminifers from the shelf to the upper slope, southern Middle Atlantic Bight. Continental Shelf Research 17, 491–508.

Buesseler, K.O., Livingston, H.D., Sholkovitz, E.R., 1985/86. ^{239,240}Pu and excess ^{240}Pb inventories along the shelf and slope of the northeast U.S. A. Earth and Planetary Science Letters 76, 10–22.

Bunt, J.A.C., Larcombe, Jago, C.F., 1999. Quantifying the response of optical backscatter devices and transmissometers to variations in particulate matter. Continental Shelf Research 19, 1199–1220.

Burrows, M., Thorpe, S.A., Meldrum, D.T., 1999. Dispersion over the Hebridean and Shetland shelves and slopes. Continental Shelf Research 19, 49–55.

Cacchione, D.A., Drake, D.E., 1986. Nepheloid layers and internal waves over continental shelves and slopes. Geo-Marine Letters 6, 147–152.

Churchill, J.H., Wirick, C.D., Flagg, C.N., Pietrafesa, L.J., 1994. Sediment resuspension over the continental shelf east of the Delmarva Peninsula. Deep-Sea Research II 41, 341–363.

Cochran, J.K., 1982. The oceanic chemistry of the uranium- and thorium-series nuclides. In: Ivanovich, M., Harmon, R.S. (Eds.), Uranium-series disequilibrium: Applications to Earth, Marine, and Environmental Sciences. Clarendon Press, Oxford, pp. 334–395.

Courp, T., Monaco, A., 1990. Sediment dispersal and accumulation on the continental margin of the Gulf of Lions: sedimentary budget. Continental Shelf Research 10, 1063–1087.

Csanady, G.T., Churchill, J.H., Butman, B., 1988. Near-bottom currents over the continental slope in the Mid-Atlantic Bight. Continental Shelf Research 8, 653–671.

De Silva, I.P.D., Imberger, J., Ivey, G.N., 1997. Localized mixing due to a breaking internal wave ray at a sloping bed. Journal of Fluid Mechanics 350, 1–27.

Dickson, R.R., McCave, I.N., 1986. Nepheloid layers on the continental slope west of Porcupine Bank. Deep-Sea Research 33, 791–818.

Duineveld, G.C.A., Lavaleye, M.S.S., Berghuis, De Wilde, P.A.W.J., Van Weele, J., Kok, A., Batten, S.D., De leeuw, J.W., 1997. Patterns of benthic fauna and benthic respiration on the Celtic continental margin in relation to the distribution of phytodetritus. Internationale Revue der gesamten Hydrobiologie 82, 395–424.

Durrieu de Madron, X., Castaign, P., Nyffeler, F., Courp, T., 1999a. Slope transport of suspended matter on the Aquitanian margin of the Bay of Biscay. Deep-Sea Research II 46, 2003–2027.

Durrieu de Madron, X., Radakovitch, O., Heussner, S., Loye-Pilot, M.D., Monaco, A., 1999b. Role of the climatological and current variability on shelf-slope exchanges of particulate matter: evidence from the Rhône continental margin (NW Mediterranean). Deep-Sea Research I 46, 1513–1538.

Emery, W.J., Thomson, R.E., 1998. Data Analysis Methods in Physical Oceanography. Pergamon Press, Oxford, UK.

Eriksen, C.C., 1998. Internal wave reflection and mixing at Fieberling Guyot. Journal of Geophysical Research 103 (C2), 2977–2994.

Gerkema, T., 1996. A unified model for the generation and fission of internal tides in a rotating ocean. Journal of Marine Research 54, 421–450.

Goericke, R., Fry, B., 1994. Variations of marine plankton δ^{13}C with latitude, temperature, and dissolved CO_2 in the world ocean. Global Biogeochemical Cycles 8, 85–90.

Holloway, C.F., Cowen, J.P., 1997. Development of a scanning confocal laser microscopic technique to examine the structure and composition of marine snow. Limnology and Oceanography 42, 1340–1352.

Holm-Hansen, O., Lorenzen, C.J., Holmes, R.W., Strickland, J.D.H., 1965. Fluorometric determination of chlorophyll. Journal du Conseil permanent pour l'Exploration de la Mer 30, 3–15.

Huthnance, J.M., 1986. The Rockall slope current and shelf-edge processes. Proceedings of the Royal Society of Edinburgh 88B, 83–101.

Huthnance, J.M., 1995. Circulation, exchange and water masses at the ocean margin: the role of physical processes at the shelf edge. Progress in Oceanography 35, 353–431.

Lohse, L., Helder, W., Epping, E.H.G., Balzer, W., 1998. Recycling of organic matter along a shelf-slope transect across the N. W. European continental margin (Goban Spur). Progress in Oceanography 42, 77–110.

Lueck, R.G., Mudge, T.D., 1997. Topographically induced mixing around a shallow seamount. Science 276, 1831–1833.

Maas, L.R.M., Benielli, D., Sommeria, J., Lam, F.-P.A., 1997. Observation of an internal wave attractor in a confined, stably stratified fluid. Nature 388, 557–561.

MacIntyre, S., Alldredge, A.L., Gotschalk, C.C., 1995. Accumulation of marine snow at density discontinuities in the water column. Limnology and Oceanography 40, 449–468.

Monaco, A., Biscaye, P., Soyer, J., Pocklington, R., Heussner, S., 1990. Particle fluxes and ecosystem response on a continental margin: the 1985–1988 Mediterranean ECOMARGE experiment. Continental Shelf Research 10, 809–839.

Monaco, A., Durrieu de Madron, X., Radakovitch, O., Heussner, S., Carbonne, J., 1999. Origin and variability of downward biogeochemical fluxes on the Rhône continental margin (NW Mediterranean). Deep-Sea Research I 46, 1483–1511.

Oey, L.-Y., 1998. Eddy energetics in the Faroe-Shetland channel: a model resolution. Continental Shelf Research 17, 1929–1944.

Puig, P., Palangues, A., 1998. Nepheloid structure and hydrographic control on the Barcelona continental margin, northwestern Mediterranean. Marine Geology 149, 39–54.

Sheldon, R.W., 1972. Size separation of marine seston by membrane and glass-fiber filters. Limnology and Oceanography 17, 494–498.

Sherwin, T.J., 1991. Evidence of a deep internal tide in the Faeroe-Shetland Channel. In: Parker, B.P. (Ed.), Tidal Hydrodynamics. Wiley Interscience, Chichester, pp. 469–488.

Sinha, B., Pingree, R.D., 1997. The principal lunar semidiurnal tide and its harmonics: baseline solutions for M_2 and M_4 constituents on the North-West European Continental Shelf. Continental Shelf Research 17, 1321–1365.

Soetaert, K., Herman, P.M.J., Middelburg, J.J., Heip, C., De Stigter, H.S., Van Weering, Tj.E., Epping, E., Helder, W., 1996. Modeling ^{210}Pb-derived mixing activity in ocean margin sediments: diffusive versus nonlocal mixing. Journal of Marine Research 54, 1207–1227.

Stephens, M.P., Kadko, D.C., Smith, C.R., Latasa, M., 1997. Chlorophyll-a and pheopigments as tracers of labile organic carbon at the central equatorial Pacific seafloor. Geochimica et Cosmochimica Acta 61, 4605–4619.

Stoker, M.S., Harland, R., Graham, D.K., 1991. Glacially influenced basin plain sedimentation in the southern Faeroe-Shetland Channel, northwest United Kingdom continental margin. Marine Geology 100, 185–199.

Stoker, M.S., Hitchen, K., Graham, C.C., 1993. The geology of the Hebrides and West Shetland shelves, and adjacent deep-water areas. United Kingdom Offshore Regional Report, British Geological Survey, London, UK.

Tahey, T.M., Duineveld, G.C.A., Berghuis, E.M., Helder, W., 1994. Relation between sediment–water fluxes of oxygen and silicate and faunal abundance at continental shelf, slope and deep-water stations in the northwest Mediterranean. Marine Ecology Progress Series 104, 119–130.

Thomsen, L., Van Weering, T.C.E., 1998. Spatial and temporal variability of particulate matter in the benthic boundary layer at the N. W. European continental margin (Goban Spur). Progress in Oceanography 42, 61–76.

Thomson, J., Colley, S., Anderson, R., Cook, G.T., MacKenzie, A.B., 1993. Pb in the sediments and water column of the Northeast Atlantic from 47 to 59°N along 20°W. Earth and Planetary Science Letters 115, 57–87.

Thorpe, S.A., 1987. Current and temperature variability on the continental slope. Philosophical Transactions of the Royal Society London A 323, 471–517.

Thorpe, S.A., White, M., 1988. A deep intermediate nepheloid layer. Deep-Sea Research 35, 1665–1671.

Turrell, W.R., Slesser, G., Adams, R.D., Payne, R., Gillibrand, P.A., 1999. Decadal variability in the composition of Faroe Shetland Channel Bottom Water. Deep-Sea Research I 46, 1–25.

Van Aken, H.M., 1988. Transports of water masses through the Faroese Channels determined by an inverse method. Deep-Sea Research 35, 595–617.

Van Aken, H.M., Eisma, D., 1987. The circulation between Iceland and Scotland derived from water mass analysis. Netherlands Journal of Sea Research 21, 1–15.

Van Weering, T.C.E., McCave, I.N., De Stigter, H.C., Hall, I., Thomsen, L., 1998. Recent sediments, sediment accumulation and carbon burial at Goban Spur, N. W. European continental margin (47-50°N). Progress in Oceanography 42, 5–35.

Verardo, D.J., Froelich, P.N., McIntyre, A., 1990. Determination of organic carbon and nitrogen in sediments using the Carlo-Erba NA-1500 analyzer. Deep-Sea Research 37, 157–165.

Walsh, J.J., Biscaye, P.E., Csanady, G.T., 1988. The 1983–1984 Shelf Edge Exchange Processes (SEEP-I) experiment: hypotheses and highlights. Continental Shelf Research 8, 435–456.

Wollast, R., 1991. The coastal organic carbon cycle: fluxes, sources and sinks. In: Mantoura, R.F.C., Martin, J.-M., Wollast, R. (Eds.), Ocean Margin Processes and Global Change. Wiley Interscience, Chichester, pp. 365–381.